NO$_x$ and O$_3$ above a tropical rainforest: an analysis with a global and box model

R. C. Pike[1], J. D. Lee[2], P. J. Young[1,3,4], G. D. Carver[1,5], X. Yang[1], N. Warwick[1], S. Moller[6], P. Misztal[7,8], B. Langford[9], D. Stewart[10,*], C. E. Reeves[10], C. N. Hewitt[9], and J. A. Pyle[1,5]

[1]Centre for Atmospheric Science, Department of Chemistry, University of Cambridge, Lensfield Road, Cambridge, CB2 1EW, UK
[2]National Centre for Atmospheric Science (NCAS), University of York, Heslington, York, YO10 5DD, UK
[3]Cooperative Institute for Research in the Environmental Sciences, University of Colorado, Boulder, CO, USA
[4]NOAA Earth System Research Laboratory, Boulder, CO, USA
[5]National Centre for Atmospheric Science - Climate, University of Cambridge, USA
[6]Department of Chemistry, University of York, Heslington, York, YO10 5DD, UK
[7]Centre for Ecology and Hydrology Edinburgh, Bush Estate, Penicuik, Midlothian, EH26 0QB, UK
[8]The University of Edinburgh, School of Chemistry, Joseph Black Building, West Mains Road, Edinburgh, EH9 3JJ, UK
[9]Lancaster Environment Centre, Lancaster University, Lancaster, LA1 4YQ, UK
[10]School of Environmental Sciences, University of East Anglia, Norwich, NR4 7TJ, UK
*now at: Department of Chemistry, University of Reading, Whiteknights, Reading, RG6 6AH, UK

Abstract. A cross-platform field campaign, OP3, was conducted in the state of Sabah in Malaysian Borneo between April and July of 2008. Among the suite of observations recorded, the campaign included measurements of NO$_x$ and O$_3$– crucial outputs of any model chemistry mechanism. We describe the measurements of these species made from both the ground site and aircraft. We then use the output from two resolutions of the chemistry transport model p-TOMCAT to illustrate the ability of a global model chemical mechanism to capture the chemistry at the rainforest site. The basic model performance is good for NO$_x$ and poor for ozone. A box model containing the same chemical mechanism is used to explore the results of the global model in more depth and make comparisons between the two. Without some parameterization of the nighttime boundary layer – free troposphere mixing (i.e. the use of a dilution parameter), the box model does not reproduce the observations, pointing to the importance of adequately representing physical processes for comparisons with surface measurements. We conclude with a discussion of box model budget calculations of chemical re-

action fluxes, deposition and mixing, and compare these results to output from p-TOMCAT. These show the same chemical mechanism behaves similarly in both models, but that emissions and advection play particularly strong roles in influencing the comparison to surface measurements.

1 Introduction

A four month field campaign, part of the NERC-funded "Oxidant and Particle Photochemical Processes" (OP3)[1], was conducted in the Malaysian state of Sabah, on the island of Borneo, between April and July of 2008 (Hewitt et al., 2010). There were two intensive periods of observation: the first between 8 April and 3 May, and the second between 25 June and 23 July. A key goal of the project is to assess our understanding of photochemical processes above a rainforest and their impacts on various scales; to this end, the campaign utilized simultaneous ground, airborne, and satellite measurements[2]. A further aim is to understand the scale relationships

---

[1]More information on OP3 can be found online at: http://www.es.lancs.ac.uk/op3/

[2]For a full list of instrumentation see Hewitt et al. (2010).

of these measurements as they are used by and contribute to mesoscale, regional, and global models.

Atmospheric oxidation above a tropical rainforest is complex (e.g. Kuhn et al., 2007; Ganzeveld et al., 2008; Lelieveld et al., 2008), and it is therefore beyond current computational resources to represent it explicitly in a global model. Furthermore, the horizontal resolution of the current generation of global models is 2–5° (approximately equivalent to 220 and 550 km at the equator) (Stevenson et al., 2006), that limits their ability to model processes that occur at the subgrid scale, such as emission variability and the influence of local topography. At the same time, these models are designed to to simulate the production and destruction of ozone, which is dependent on local chemical conditions (Crutzen, 1973; Sillman et al., 1990; Jenkin and Clemitshaw, 2000). Ozone is important for radiation (Gauss et al., 2006), and at high concentrations is detrimental to both human (Wilkins et al., 2001; Jerrett et al., 2009) and crop health (van Dingenen et al., 2009). Our understanding of the future impacts of ozone very often relies on the output of global models (Forster et al., 1996; Fuglestvedt et al., 1999; Stevenson et al., 2006) and it is therefore essential to understand how global chemical mechanisms perform in relation to the local measurements which help to constrain them.

Production of tropospheric ozone is a non-linear function of its precursor concentrations (Liu et al., 1987; Jenkin and Clemitshaw, 2000), and depends largely on local concentrations of volatile organic compounds (VOC), the hydroxyl radical (OH), and the oxides of nitrogen (NO + NO$_2$ = NO$_x$) (e.g. Sillman, 1995). NO and NO$_2$ act as catalysts in many oxidation cycles in the atmosphere due to their rapid interconversion; the availability of NO$_x$ largely determines whether ozone production or destruction dominates in a specific region of the tropical boundary layer (Liu et al., 1987; Trainer et al., 1991). The impact of NO$_x$ on ozone production in the OP3 observation region has been previously described (Hewitt et al., 2009).

Photolysis of NO$_2$ is the largest known production mechanism for ozone in the troposphere, while loss occurs through photochemical reaction with other trace gases and deposition to surfaces such as the ocean or vegetation. Ozone can also be entrained into the troposphere from the ozone-rich stratosphere (Holton et al., 1995). The lifetime of tropospheric ozone can range from a few days to over a month, depending on location in the atmosphere (e.g. Stevenson et al., 2006; Wild, 2007). Transport from the free troposphere may therefore influence local boundary layer measurements of ozone.

The odd oxygen (O$_x$ = O$_3$ + NO$_2$) budget is described by:

$$\frac{d[O_x]}{dt} = k_{prod}[O_x] - k_{loss}[O_x] + k_{mixing}\delta[O_x] - k_{dep}[O_x] \quad (1)$$

where the terms represent chemical production, chemical loss, mixing (transport), and deposition, respectively. For the mixing term, $\delta[O_x]$ represents the vertical gradient. Chemi-

cal production of odd oxygen is dominated by the oxidation of NO to NO$_2$ by peroxy radicals:

$$k_{prod}[O_x] = k_a[NO][HO_2] + k_b[NO][RO_2] \quad (2)$$

where RO$_2$ is a generic hydrocarbon peroxy radical. O$_x$ chemical loss is represented by:

$$k_{loss}[O_x] = k_c[O_3][HO_2] + k_d[O(^1D)][H_2O] + k_e[O_3][alk.] \quad (3)$$

where alk. represents a generic alkene (e.g. isoprene). An additional term to the chemical loss is oxidation of NO$_2$ to other nitrogen species, such as nitric acid.

The NO budget can be described in a similar fashion to ozone in Eq. (1), and the ratio between NO and NO$_2$ can be expressed as:

$$\frac{[NO]}{[NO_2]} = \frac{j_{NO_2}}{k_f[O_3] + k_a[HO_2] + k_b[RO_2]} \quad (4)$$

Nitrogen oxides are emitted both by natural processes and human activities. Of the natural sources, emission from soils (Yienger and Levy II, 1995; Delon et al., 2008) and formation during lightning storms (Franzblau and Popp, 1989; Schumann and Huntrieser, 2007) are the major contributors. Although fluxes from tropical areas are not yet well constrained, the work of Bakwin et al. (1990) suggested significant emissions from tropical forested areas. Jaeglé et al. (2004) reported that soil emissions could be as large as biomass burning emissions in Africa. Fossil fuel combustion, biomass burning and aircraft emissions are the major anthropogenic sources (Kasibhatla, 1993; Levy II et al., 1999; Toenges-Schuller et al., 2006). In these remote tropical areas the potential for NO$_x$ species to influence local chemistry is significant due to low background NO$_x$ and high concentrations of both the hydroxyl radical and biogenic VOC (Steinkamp et al., 2009). An increase in the frequency and spatial distribution of tropical NO$_x$ measurements will help quantify local tropical fluxes and sources. Global models can be used to quantify the impact of these fluxes on a regional and global scale. For this reason, it is important to understand how well global models validate against local scale measurements, and how the approximations of physical and chemical processes affect the comparison.

This study consists of two parts. The first part presents the measurements of NO, NO$_2$, and ozone taken over the two four-week periods at the OP3 remote rainforest location, from ground and aircraft platforms. In the second part, results from a global chemical transport model (CTM) are presented, and the comparison to the observations assessed. Results from a box model, using the same chemical mechanism as the CTM, are then used to explore the potential physical and chemical factors important to the observations, followed by a detailed ozone budget analysis to assess what drives the differences between the two models.

The paper is organized as follows: Sect. 2 presents a summary of the measurement techniques and the observations. Section 3 details the comparison between the measurements in two different chemical modelling frameworks.

In Sect. 3.1, the Cambridge p-TOMCAT CTM is integrated at two different horizontal resolutions. In Sect. 3.2, the box model results are compared to the measurements and p-TOMCAT, and then used to explore the budget of ozone. Finally, Sect. 4 summarizes the study and the results.

2 Measurements

2.1 Methods

Nitrogen oxides and ozone measurements were taken at the Bukit Atur Global Atmospheric Watch (GAW) station ($04°58'53''$, $117°50'37''$, and elevation 426 m). NO measurements were made by chemiluminescence using an Ecophysics CLD 780 TR nitric oxide analyzer, with an Ecophysics PLC 762 NO₂ photolytic converter connected to allow conversion of NO₂ to NO. NO and NO₂ concentrations were measured from an inlet situated at 5 m above ground level through quarter-inch PFA tubing. Measurements were run on continuous sampling except during calibrations and when running NOₓ-free air. The analyzer was calibrated using an Eco Physics PAG003 pure air generator, an Environs calibration gas blender S6100 and a cylinder of 450 ppbv NO in nitrogen. The photolytic converter efficiency is also determined as part of the calibration. NOₓ-free air was run through the system on several occasions to allow more accurate determination of the systematic artefact and detection limit.

Each measurement cycle lasted for 1 min and consisted of 12 s of NO measurement, 12 s of NO₂ measurement and 24 s of interference determination. The remaining 12 s allowed for switching between the different modes and purging of the reaction cell. The 1σ limit of detection for 10 min frequency data was approximately 2.8 pptv for NO and 7 pptv for NO₂.

Ozone concentrations were measured using a Thermo Environmental Instruments (TEI) 49i UV absorption ozone analyzer. The data was internally averaged to one minute frequency and the detection limit was 0.6 ppbv.

Groundbased measurements were made during both intensive measurement periods of OP3. In June and July 2008, the campaign was complemented by airborne measurements. On board the Facility for Airborne Atmospheric Measurements (FAAM) BAe 146 aircraft, NO and NO₂ were measured using the University of East Anglia (UEA) NOxy instrument, which employed the same technique as the ground based instrument described above. Interference determinations were carried out at the beginning of level runs during the flights and calibrations took place during transit to and from the airport. Detection limits of the UEA NOxy are on the order of 3 pptv for NO and 15 pptv for NO₂ for 10 s data, with estimated accuracies of 10% for NO at 1 ppbv and 10% for NO₂ at 1 ppbv. The instrument is described in detail by Brough et al. (2003). Ozone was measured on board the aircraft using a TEI 49C UV absorption analyser.

Isoprene fluxes, used in the box modelling experiments, were measured using a PTR-MS instrument at the Bukit Atur site. Its response was optimized so as to achieve the best compromise between the optimal detection limit for VOCs and the minimization of the impact of high relative humidity. The operational details of the instrument have been presented elsewhere (e.g Lindinger et al., 1998; de Gouw et al., 2003; Blake et al., 2009) and the experimental setup and methodology for OP3 will be described in a forthcoming paper (Langford, et al., Fluxes of volatile organic compounds from a south-east Asian tropical rainforest, 2009. This special issue, in prep.). High frequency temperature data, also used as input to the box model, were obtained from a 20-Hz sonic anemometer (Windmaster Pro, Gill Instruments Ltd.), which was collocated with the sampling inlet for PTR-MS.

2.2 NO, NO₂, and O₃ results

Figure 1 shows the time series of NO, NO₂, and O₃ measurements. Although the frequency of data collection is 1 min (Sect. 2.1), it is shown here with a running average of 10 minutes for smoothing purposes. NO levels were typically below 0.1 ppbv, although there were regular spikes above this level that reached up to 0.4 ppbv. NO₂ levels were higher, generally below 0.4 ppbv but reaching 0.8 ppbv. Ozone concentrations ranged from near zero up to 30 ppbv, but were only consistently above 20 ppbv on three days (11–13 April).

Figure 2 shows the median diurnal profiles for the entire April measurement period for all three species[3]. The 25–75 inter-quartile range is shown in shaded regions around each of the profiles. The ozone diurnal cycle shows a minimum of approximately 6 ppbv around 07:00 h followed by a rise through the morning. Ozone concentrations of approximately 11 ppbv remain until the evening, when concentrations slowly fall to their minimum in the morning. NO₂ concentrations exhibit the most amplified diurnal cycle, which peaks at midnight around 240 pptv and reaches a low of 80 pptv in mid-afternoon. The loss of NO₂ between midnight and midday occurs less rapidly than the buildup between late afternoon and evening. An NO peak of around 70 pptv is observed at 08:00 h and quickly recovers to a fairly constant level between 30 and 40 pptv. This persists until 18:00 h when a further drop to 20 pptv occurs. Non-zero NO concentrations between 15–20 pptv persist throughout the night.

In July, an aircraft joined the campaign in order to make dedicated measurements above the site and over the surrounding areas. On the right side of Fig. 2, the diurnal cycles of NO, NO₂, and O₃ from the ground site at the Bukit Atur GAW tower are shown for this second observation period. These diurnal cycles were sampled only for the four days for which equivalent aircraft data are also available. The average

---

[3]A version of this Figure appeared in Hewitt et al. (2010). The Figure that appears here has higher temporal resolution (10 min data) than the previous version (1 h data).
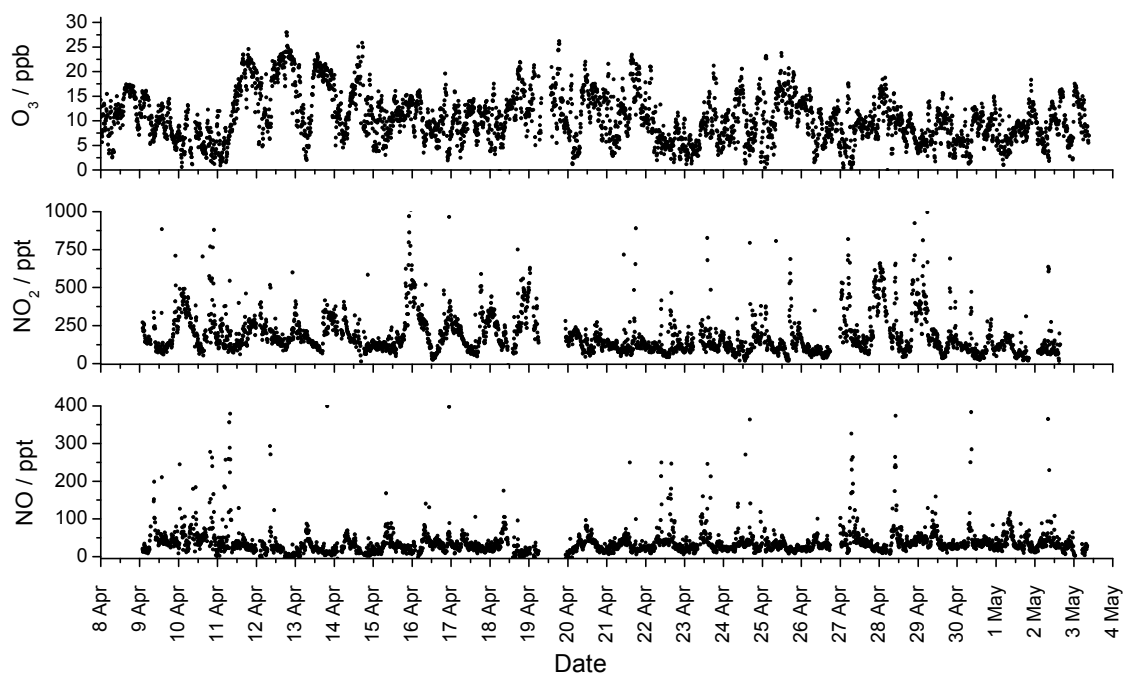
Fig. 1. Time series of measured NO, NO₂, and O₃ at the Bukit Atur GAW ground site, plotted versus local time (GMT+8).
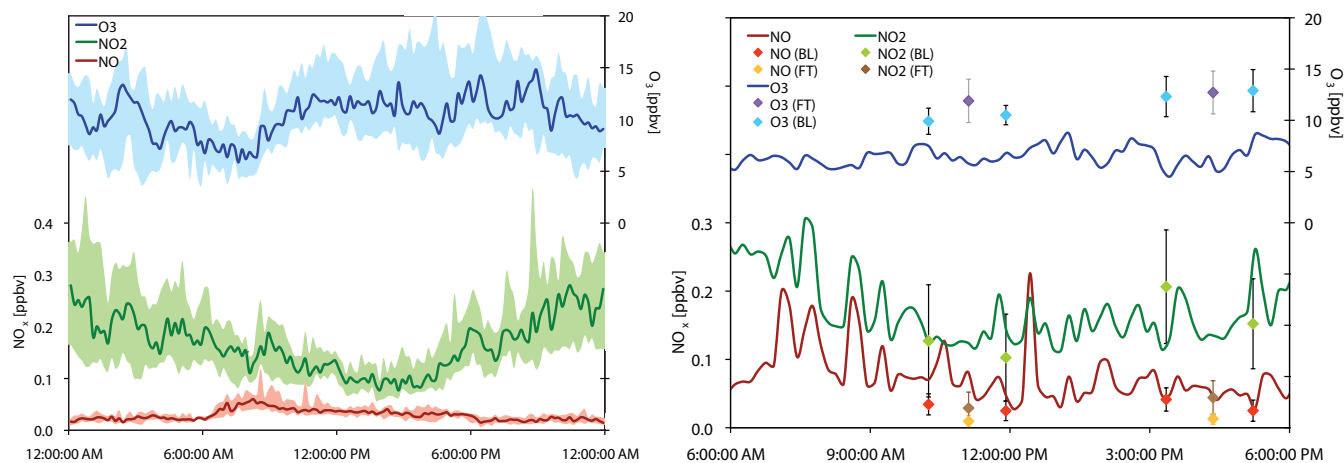
Fig. 2. Left: Median diurnal cycle of ground-based measured NO (dark red), NO₂ (dark green), and O₃ (dark blue) in April. The corresponding 25–75 quartile interval is shown with each measurement: NO in pink, NO₂ in light green, and O₃ in light blue. Right: median diurnal measurements in July, shown only for the days when corresponding flight data is available between 06:00 and 18:00 h; diurnal profiles are the same color. Average flight data for morning and afternoon profiles above the site are shown as whiskered points and are separated by height. NO boundary layer measurements are show in red (boundary layer) and yellow (free troposphere). NO₂ is shown in light green (boundary layer) and brown (free troposphere). O₃ is shown in light blue (boundary layer) and purple (free troposphere).

measurements made in profile flight patterns directly over the site are plotted as whiskered points (again with the 25–75% inter-quartile range) and show values for both boundary layer and free troposphere.

The aircraft data show that ozone had very little vertical gradient; the boundary layer and free tropospheric values are nearly identical. A diurnal structure in the ground based

O₃ observations in July is not clear, with the values around 9 ppbv. The ground based and aircraft measurements show a slight discrepancy (9 ppbv versus 11 ppbv), most likely due to dry deposition occuring near the Bukit Atur site.

Boundary layer NO₂ matches the ground-based measurements closely, the latter remaining in the range of 100–200 pptv for most of the day. Aircraft NO₂ measurements

show a similar structure (rise until midnight and subsequent decrease afterwards) to the first campaign, but because only four days are sampled here the full diurnal cycle is not shown. Aircraft NO_2 measurements in the free troposphere (20 pptv) were much lower than those in the boundary layer and at the surface, demonstrating that NO_2 had a strong vertical structure. The difference is between 80% and 90%.

NO displays a similar pattern to NO_2, with boundary layer values that resembled ground-based measurements well, and free tropospheric values that were much lower (less than 10 pptv compared to 80–200 pptv). The diurnal cycle of NO also bears resemblance to that of the first campaign, (i.e. a rise in early morning followed by a slow tapering into the afternoon).

For comparison, the NO concentrations at the ground site in both measurement periods were in between measurements made in the Amazon Rainforest of 20 pptv (Lelieveld et al., 2008) and 100 pptv (Karl et al., 2009). Ozone, on the other hand, was lower at the Borneo site than in reported values for the Amazon for both the boundary layer (19 ppbv) and the free troposphere (37 ppbv) (Lelieveld et al., 2008).

3 Model simulations

In this section two sets of model simulations are described. Section 3.1 discusses the use of a global model to simulate the diurnal cycle of the three measured species NO, NO_2, and ozone. In Sect. 3.2, we describe the use of a box model to explore the chemical and physical budget terms, and examine how these influence the mechanism's performance in replicating observations.

3.1 Global model

3.1.1 Model description

We used the Cambridge global chemistry transport model (CTM) p-TOMCAT to simulate the diurnal cycles of NO, NO_2, and O_3 observed during the April measurement period. The Cambridge p-TOMCAT global CTM is described in more detail in Cook et al. (2007) and Hamilton et al. (2008). The model was used for this study in both a high horizontal resolution mode ($0.56° \times 0.56°$, approximately 62 km in the tropics) and a low resolution mode ($2.8° \times 2.8°$, approximately 310 km in the tropics). There are 31 levels in the vertical, from the surface to 10 hPa. Over Borneo the thickness of the surface layer was about 65 m with the next layer at about 170 m. Both resolutions were driven by 6 hourly operational analyses of wind, temperature, and humidity at a horizontal resolution of 2.8° from the European Centre for Medium-range Weather Forecasting (ECMWF). The boundary layer height was diagnosed from input ECMWF operational analyses using the non-local scheme of Holtslag and Boville (1993).

The model mechanism was the same as described by Arnold et al. (2005), with the addition of the Mainz isoprene mechanism (Pöschl et al., 2000) implemented as described by Young et al. (2009) (for the UM_CAM model). It is a medium-size chemistry for a global model, simulating the oxidation of methane, ethane, propane, and isoprene, with 81 tracers and ∼200 reactions. Time dependent chemical concentrations were calculated with the ASAD package (Carver et al., 1997). Photolysis rates for 37 species are determined using offline look-up tables generated by the Cambridge 2-D model (Law and Pyle, 1993) using the multiple scattering scheme of Hough (1988). These offline rates were based on climatological cloud cover and a fixed aerosol profile.

Emissions of NO_x, CO, ethane, propane and isoprene were included based on Gauss et al. (2003). The lightning emissions were scaled to produce $5 \, Tg \, N \, yr^{-1}$ using the parameterization of Price and Rind (1992) implemented according to Stockwell et al. (1999). A seasonal variation was applied to the biomass burning emissions using the distribution of Hao and Liu (1994). Isoprene emissions were taken from the Global Emissions Inventory Activity (GEIA) of Guenther et al. (1995) with a diurnal cycle applied in the model. Note that these fluxes were about a factor three higher than the measured fluxes used in the box model (box model fluxes were taken from measurements, as described below). Dry deposition velocities were calculated according to the method of Giannakopoulos (1998) using prescribed land type-specific data based on data from Ganzeveld and Lelieveld (1995) and Zhang et al. (2003).

3.1.2 Global model results

Figure 3 shows the monthly mean diurnal variations of surface NO, NO_2, and ozone in the boundary layer. Both model resolutions show a fit for NO concentrations which matches the data well. The model reached a maximum of 65 pptv in the morning around 08:00 h, when the measurement data also peaked (at 60 pptv). At low resolution, there was a dip in midday values to 40 pptv, which was not recorded in the measurements. NO dropped to zero around 18:00 h in p-TOMCAT, coinciding with the point when measurement values also dropped. As noted in Sect. 2.2, residual NO concentrations of approximately 20 pptv were present throughout the night, and these values were not captured by the global model at either resolution.

The model-measurement comparison for NO_2 is reasonable for both p-TOMCAT resolutions, although the range of the diurnal cycle was 10% too high at 222 pptv, compared with 203 pptv in the measured data. The low resolution version of the model showed constant NO_2 concentrations at night, while the high resolution version of the model showed an increase in NO_2 until dawn. At higher altitudes in the model (not shown), NO_2 concentrations were lower (less than 50 pptv) than in the boundary layer levels, which is consistent with the observed vertical profile (Sect. 2.2). We
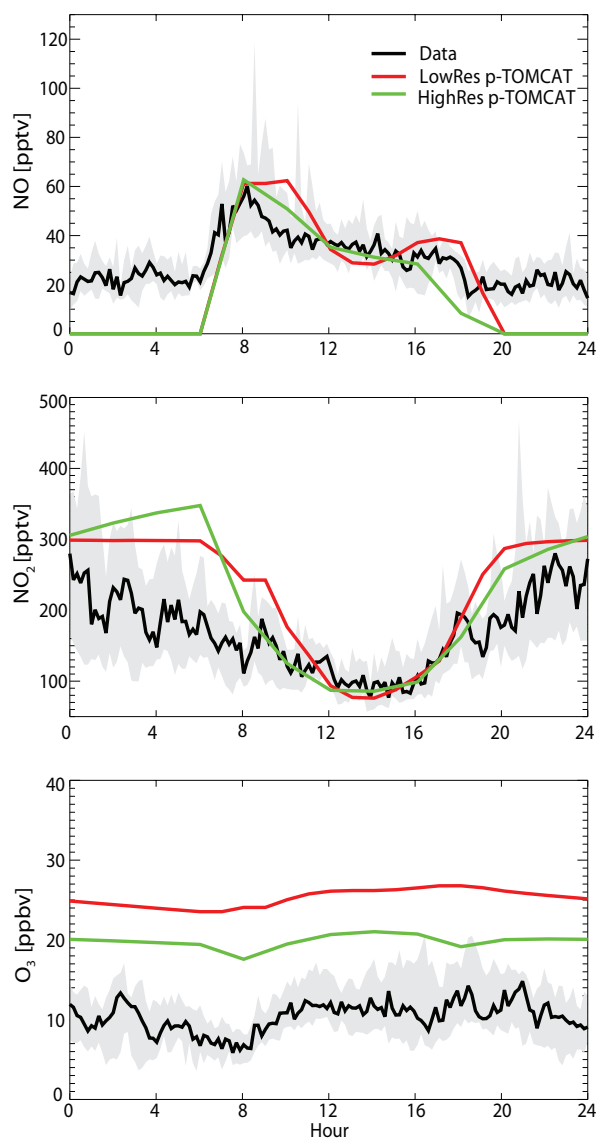
Fig. 3. Global model comparison to diurnal cycle of NO, NO$_2$, and O$_3$ from the median diurnal cycle in the measurements (black, with 25–75 quartile in grey). The global model is shown in red (low resolution) and green (high resolution) for the lowest model level.

argue below that the measurements reflect a large component of free tropospheric character due to mixing during the second half of the night (24:00 to 06:00 h). It is possible that mixing between boundary layer and free tropospheric air in the global model is not sufficient to capture the nighttime decrease in NO$_2$ shown in the measurements. In addition, the diurnal pattern in both resolutions of the model is slightly too narrow, with a more precipitous decrease in concentrations in the morning and a stronger rise in the evening. In contrast, the measurements showed a smoother rise and fall throughout the day and night. Both models capture the rise between 14:00 and 18:00 well.

Finally, the modelled ozone is too high in the global model. Concentrations in the low resolution model integration were as high as 26.8 ppbv. The higher resolution model performs slightly better with values of approximately 20 ppbv. In contrast, measured mixing ratios were between 6 and 13 ppbv. Despite this, the diurnal cycle of the model seems to capture the observed data, which shows little diurnal variation. The higher resolution integration has a more realistic representation of deposition, an important loss process for ozone, due to a higher resolution land-sea mark and improved representation of the land surface type. It also shows a much stronger land-sea gradient in ozone concentrations compared to the low resolution integration of the model (see Fig. 10 in Hewitt et al., 2010).

3.2 Box model

Using these global model results as a starting point, we employed a box model fitted with the same chemical mechanism to explore the budgets of ozone and NO$_x$.

3.2.1 Model description

The box model was used in two configurations. All the experiments and results described in the main text of the paper use the "constrained" configuration. A series of additional sensitivity studies was conducted with the box model in a second configuration, in which we altered the photolysis rate of NO$_2$ in order to account for cloud cover. We describe the "test" model configuration and those experiments in the Supplements.

Dry deposition in the constrained box model uses the same tabulated values as the global model, but only six species were deposited: NO, NO$_2$, O$_3$, peroxy acetyl nitrate (PAN), peroxy-methacrylic nitric anhydride (MPAN), and a lumped nitrate species representing the products from isoprene oxidation (ISON, see Pöschl et al., 2000). Nitric acid was not deposited as its impact on the chemistry is minimal due to its slow oxidation. Table 1 shows the deposition velocities for day and night. These closely match the deposition velocities in the p-TOMCAT model for the forest land type. The photolysis followed the scheme of the Master Chemical Mechanism (MCM, Saunders et al., 2003).

Only NO and isoprene are emitted into the box. Isoprene emissions into the model were taken from ground based flux measurements (see Fig. 9a of Hewitt et al., 2010), which were described in Sect. 2.1. In order to maintain consistency between both models, we did not include monoterpene emissions or chemistry, although monoterpene emission measurements were made (Hewitt et al., 2010). Initial reaction of a monoterpene species with OH, O$_3$, and NO$_y$ could contribute to the budgets at the site. Occasionally, isoprene flux measurements were not available due to power outages and used linear interpolation was used to fill the data gaps. We used NO emissions of 6×10^9 molec cm^2 s^{-1}, which is in

Table 1. Dry deposition velocities [cm s^{-1}] for species in the box model, which are the same as rainforest values for the global p-TOMCAT model.

Species	V_d Day	V_d Night
O$_3$	0.85	0.30
NO	0.14	0.01
NO$_2$	0.83	0.04
PAN	0.63	0.14
MPAN	0.63	0.14
ISON	1.00	0.06

Table 2. Initial concentrations of six species used in the box model.

Species	Concentration
CO	130 ppbv
H$_2$O$_2$	3 ppbv
C$_2$H$_6$	500 pptv
C$_3$H$_8$	50 pptv
HCHO	1 ppbv
CH$_3$COCH$_3$	50 pptv
CH$_4$	1700 ppbv
H$_2$	500 ppbv

between the values of Pugh et al. (2010) and Bakwin et al. (1990). This emission rate was held constant since, in the absence of NO flux measurements at the site, we were not able to constrain NO emissions to a diurnal pattern. NO flux measurements were made nearby underneath the canopy layer (Dorsey and Gallagher, 2010). However, the Bukit Atur GAW station is in a clearing, and therefore canopy flux measurements are not representative of this site: there can be a strong difference between below- and above-canopy fluxes of NO$_x$ (e.g. Duyzer et al., 2004). Constant NO emission was also consistent with the emissions used in the global model.

The box model boundary layer height was fixed to 600 m set value during the day (06:00 to 18:00 h) and to 200 m tonight at night, based on the backscatter measurements of Pearson et al. (2010). The boundary layer height is effectively a mixing depth, and therefore controlled the range over which emissions are mixed into the model, as well as the rate of sinks via deposition.

Temperature data (30 min averages) were taken from measurements made alongside the isoprene flux measurements (Sect. 2.1), and pressure was set to 950 mb in the box, appropriate to the conditions of the rainforest site (this value was also used for the back trajectories described in Sect. 2.3 of Hewitt et al., 2010).

Table 2 shows the initial concentrations of chemical species in the box model based on approximate concentrations measured during the campaign from the on site gas chromatographs (see Hewitt et al., 2010). NO, NO$_2$, and O$_3$ were initialized to their midnight values from the diurnal cycle in the measurements. All other species were initialized to zero.

For the model-measurement comparisons, both the model and the data were sampled for 15 days to account for day to day variability in isoprene flux measurements.

3.2.2 Dilution

The experiments described in the Supplement showed that the model had a much higher sensitivity to the parameterizations of physical processes than chemical ones. The param-

eter that made the single largest difference was the introduction of a dilution parameter, which is described below.

Doppler lidar measurements of the backscatter from aerosol (Pearson et al., 2010) provide strong evidence for dilution of aerosol in the boundary layer during the latter half of the night. The ground measurements were made in an area of complex topography, with the lidar measurements made in a valley at an elevation of 198 m (Pearson et al., 2010) compared with 426 m for the Bukit Atur site where the NO$_x$ and ozone measurements were conducted. At night, lidar measurements showed that the median boundary layer height dropped to approximately 200 m, suggesting that on some nights the Bukit Atur site may have effectively been in the free troposphere. To simulate this, we introduced a "dilution parameter" to the box model. This was a simple way to simulate the mixing between the boundary layer box and the free troposphere by parameterizing dilution of species which are concentrated in the boundary layer. The dilution parameter was particularly important to capture the behaviour of NO$_x$.

Figure 4 shows the impact of the dilution parameter. The dilution parameter was set to remove 2% of chemical tracers (except ozone: see below) at each 10 min timestep between 24:00 h and 06:00 h by relaxing each species to a concentration of zero, similar to the work of Biesenthal et al. (1998). The value of 2% was determined through a series of sensitivity tests performed with a "test" model (see Supplement), in which we allowed a number of parameters to be fixed, including the boundary layer height. Using this alternative configuration of the box model, we performed a cost function analysis of physical parameters. A 2% dilution per timestep is approximately equivalent to a 50% reduction in concentration during the period of dilution (6 h), or a 95% reduction over a 24 h period.

The dilution parameter simulates exchange with free tropospheric air at night and assumes that this incoming air has lower concentrations of NO and NO$_2$. O$_3$, however, displayed little vertical gradient in the aircraft measurements (see Fig. 2), and so is not diluted. Not diluting O$_3$ is the numerical equivalent of removing O$_3$ and introducing an equal

amount during the same amount of time, such that a collapse of the boundary layer and mixing with the free tropospheric air may well bring in "new" ozone, but the concentrations will be similar to the boundary layer air it is replacing. This methodology is reinforced by the difference between the species in their distribution of sources and sinks; NO_x has a source which is largely surface dominated at a remote rainforest location (higher in the troposphere, lightning can contribute as well), whereas ozone has a significant surface sink due to deposition.

Figure 4 shows that NO measurements and model simulations were in fairly good agreement following the addition of the dilution parameter. The buildup of NO_2 until midnight and subsequent reduction in concentrations was well captured. At sunrise, when the boundary layer begins to grow, a steep drop in NO_2 concentrations appeared around 06:00 h in the box model due to the onset of photolysis. The largest divergence between modelled and measured values occurred in the afternoon, between 12:00 and 16:00 h. Base case modelled and measured ozone displayed similar diurnal cycles. Both show minima between 07:00 h and 08:00 h and maxima in the late afternoon, though the measurements had more structure in the afternoon than the modelled ozone. Ozone showed a change with dilution due to its chemical relationship with NO and NO_2.

3.2.3 Budget calculations

O_x budget diagnostics were implemented into both the box model and the high resolution version of p-TOMCAT in order to investigate the relative contributions of chemistry, mixing, and deposition. The goal was also to investigate the differences in the ozone, NO, and NO_2 concentrations simulated by the box and global models.

Table 3 shows the daily integrated fluxes through the key chemical reactions for the O_x budget for both models, as well as the contribution from deposition and mixing (box model) and advection (p-TOMCAT). In order to make a fair comparison between the models, the p-TOMCAT budget was calculated over the levels comprising the model's representation of the boundary layer (four model levels during the day and two at night).

For O_x, chemical production was dominated by the reaction between HO_2 and NO accounting for approximately 45% (box model) or 40% (p-TOMCAT) of total chemical production. Individual NO + RO_2 terms for the box model show that the reaction of NO with the isoprene peroxy radical (ISO2, representing all possible isomers from the reaction of isoprene and OH) had the next largest flux, greater than 2 ppbv day^{-1}, followed by nearly equal contributions from the methyl peroxy radical, the acetyl radical, and MACRO2 (peroxy radicals from the second generation isoprene products). Production of NO_2 via oxidation and photolysis of nitrates (equivalent to NO to NO_2 conversion), and produc-
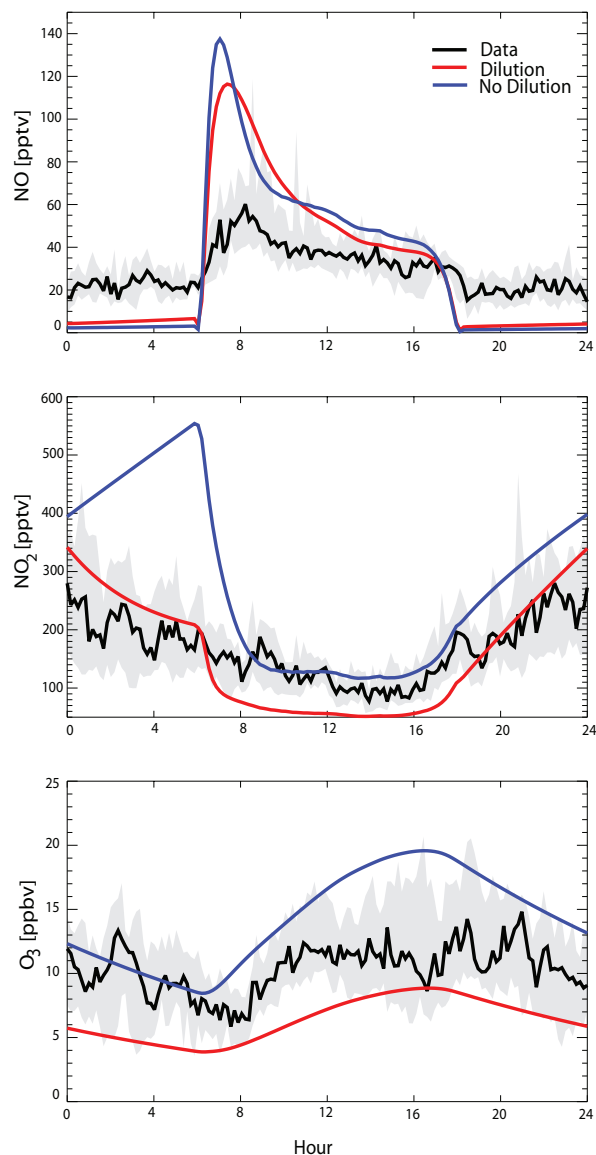
Fig. 4. Box model comparison with (red) and without (blue) venting against diurnal cycle of NO, NO₂, and O₃ from the median diurnal cycle in the measurements (black, with 25–75 quartile in grey).

tion of ozone from the reaction of acyl peroxy radicals with HO_2, was negligible.

For p-TOMCAT, the flux through the NO + CH_3O_2 reaction was nearly double that of the box model. Furthermore, the p-TOMCAT NO + RO_2 flux (where RO_2 is all peroxy radicals except HO_2 and CH_3O_2) was 30% greater than the equivalent box model. Overall, the chemical production term was over 20% greater in p-TOMCAT compared to the box model.

In terms of chemical loss of O_x Table 3 shows that the integrated fluxes were generally 3–6 times greater for p-TOMCAT compared to the box model, on account of the

Table 3. Budget statistics for integrated O$_x$ in [pptv day^{-1}]. Values not reported are shown as N/R, values not applicable are shown as N/A, and * indicates that N/R represents a sum of the fluxes.

Production	Box	p-TOMCAT	Loss	Box	p-TOMCAT
NO + HO$_2$	4672	5005	O(^{1}D) + H$_2$O	817	3112
NO + CH$_3$O$_2$	880	1632	O$_3$ + HO$_2$	163	1036
NO + CH$_3$C(O)O$_2$	961	N/R	O$_3$ + OH	31	44
NO + ISO$_2$	2372	N/R	O$_3$ + alkene	289	969
NO + MACRO$_2$	1026	N/R	NO$_2$ mixing	357	N/R
NO + other RO$_2$	0	6227*	O$_3$ deposition	8002	14 141
CH$_3$C(O)O$_2$ + HO$_2$	34	N/R	NO$_2$ deposition	64	N/R
Nitrate recycling of NO$_2$	19	N/R	Loss to NO$_y$	267	N/R
Net advection O$_3$	N/A	7741			
Total	9964	20 245	Total	9990	161 737

Table 4. Budget statistics for integrated NO in [pptv day^{-1}].

| Production	Flux	Loss	Flux
NO$_2$ + hν	15 906	NO + O$_3$	6670
Other chem. prod.	42	NO + HO$_2$	4672
NO emission	743	NO + CH$_3$O$_2$	881
		NO + CH$_3$C(O)O$_2$	961
		NO + ISO$_2$	2481
		NO + MACRO$_2$	1026
		NO + other RO$_2$	0
		NO mixing	7
		NO deposition	6
		Other chem. loss	51
Total	16 691	Total	16 755

higher ozone concentrations (Fig. 3). Loss in both models was dominated by the reaction of O(^{1}D) with water vapour. In the box model, direct reaction of ozone with alkenes (isoprene and the lumped C4-carbonyl species MACR) was the next most dominant loss mechanism, followed by O$_3$ + HO$_2$. The relative importance of these reactions was reversed in p-TOMCAT, although their contribution to the overall loss was broadly similar. The box model statistics show that the net loss of NO$_2$ to oxidized NO$_y$ species (e.g. nitric acid) was roughly the same as the loss to reaction with alkenes; this statistic was not available for p-TOMCAT.

Despite the differences in the fluxes, net chemical production (P-L) was roughly the same in both models: 8.4 ppbv day^{-1} in the box model and 7.5 ppbv day^{-1} in p-TOMCAT.

Differences between the box model and p-TOMCAT become more apparent when the physical terms are considered, i.e. deposition and mixing/advection. Table 3 shows that there was a substantial source of ozone from advection in p-TOMCAT, of the same order as the net chemical production. This extra source was missing from the box model, whose closest equivalent was a small loss of O$_x$ via the dilution parameter at night. The extra influx of ozone, coupled with a higher chemical source term, drives the increased deposition (approximately a factor of 2) and chemical loss (approximately a factor of 3) in p-TOMCAT, compared to the box model. Dry deposition was by far the largest contribution to total loss in both models. Furthermore, the deposition velocity of ozone was the strongest sensitivity of a number of chemical parameters in the "test" box model (see Supplement).

Figure 5 shows the diurnal cycles of the chemical production and loss, and mixing/advection and deposition terms for the box model (solid lines) and p-TOMCAT (dashed lines). The black net tendency line shows the net affect of all the terms on the O$_x$ budget: (chemical production + advection) minus (chemical loss + deposition + mixing), where advection applies only to p-TOMCAT and mixing only to the box model.
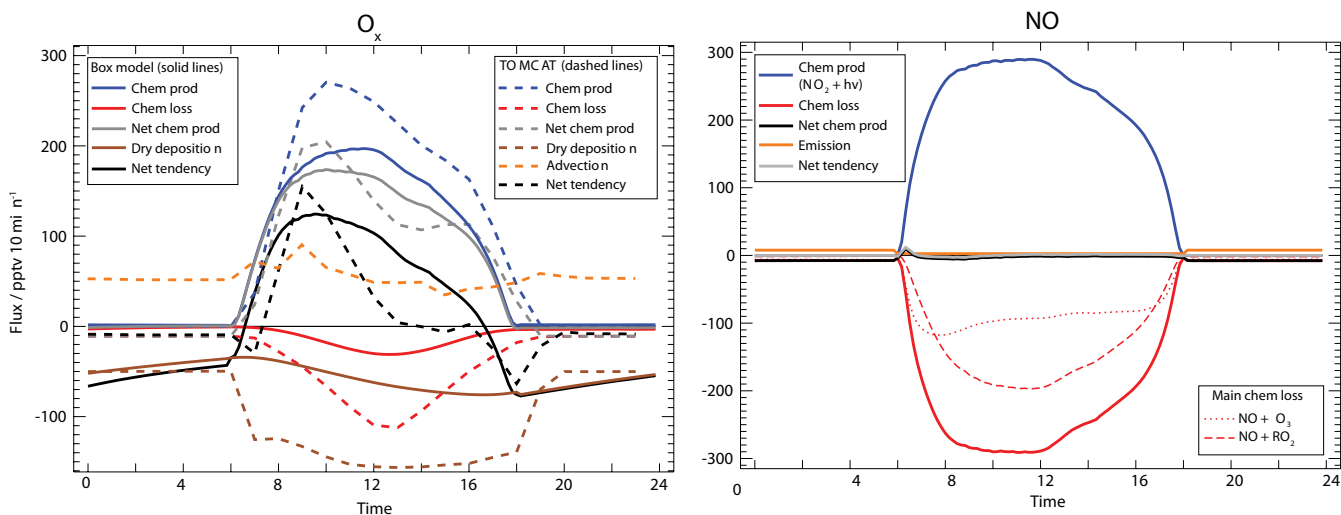
Fig. 5. Time series of production and loss of O$_X$ (left) and NO (right) throughout the day. For both, production is shown in blue, loss is shown in red, and net production is shown in black, and fluxes which make large contributions to the total budget are shown in dashed lines, each of which is indicated in the legend.

The shape of the time evolution of the chemical terms is broadly similar for both models, although reaching higher (absolute) values in p-TOMCAT as shown in Table 3. Net chemical production (grey lines) is similar, although the p-TOMCAT curve shows greater chemical production than the box in the morning, and then reduces to below the box model value in the afternoon. Both models show that loss of O$_X$ was dominated by deposition throughout the diurnal cycles.

The diurnal cycle of the net tendency curves in Fig. 5 indicates the advection term is why p-TOMCAT maintained consistently greater ozone concentrations (Fig. 3) than the box model (Fig. 4). At night the advection term balanced the dry deposition in p-TOMCAT, resulting in a near steady state for ozone concentrations. In contrast, deposition in the box model did not balance another term, resulting a negative ozone tendency. This is reflected in the diurnal shape of the ozone concentration profiles in Figs. 3 and 4, where the box model ozone concentration fell off at night, and remained largely constant in p-TOMCAT. However, the measurements suggest that ozone concentrations were relatively constant, unlike the more sinusoidal diurnal cycle of the box model. The p-TOMCAT budget statistics suggest that a net advection source of ozone is a potential candidate to explain this feature of the diurnal cycle.

As mentioned in Sect. 3.1.1, an important difference between the box model and p-TOMCAT was the magnitude of the isoprene and NO$_X$ emissions used. In p-TOMCAT, isoprene emissions were approximately a factor of two greater than the box model, and NO$_X$ emissions a factor of four greater (note "NO$_X$" was emitted as NO in the box model and NO$_2$ in p-TOMCAT). A sensitivity study was conducted where the box model isoprene and NO emissions were increased by these factors. Results from this run (not

shown) showed ozone concentrations peaking closer to the p-TOMCAT values (approximately 20 ppbv), although the daily integrated chemical production and loss terms were respectively a factor of three and two higher in this "high emission" box run, compared to p-TOMCAT.

Clearly, the differences between the simulated ozone concentrations in the box model and the p-TOMCAT surface grid cell located over Danum are related to both the details of the emissions and the treatment of the physical processes. The emissions appear to control the overall concentration, and the physical processes seemingly dominate the shape of the diurnal profile; the latter was also found by Pugh et al. (2010).

4 Conclusions

The data collected during the NERC OP3 field campaign in Sabah, Borneo, provide an opportunity to explore the questions of model validation, namely: how well can a global model chemical mechanism capture the detailed measurements? We used new ground and aircraft data of NO, NO$_2$, and ozone to address this, comparing these measurements against results from the global chemistry transport model p-TOMCAT, and a box model that included the same chemical mechanism.

The global model displayed a reasonable comparison with the diurnal patterns of NO and NO$_2$, but simulated much higher concentrations of O$_3$. The reasons for the poorer ozone comparison were investigated using a box model. This model was constrained with available observations of physical and chemical data (e.g. boundary layer height, temperature, isoprene fluxes), as well as parameterizing the impact of the nocturnal collapse of the boundary layer on species'

concentrations through a dilution parameter (see Supplement). Results from the box model generally compared well with the measured NO, NO$_2$, and O$_3$ concentrations, although the early morning increase in NO was overestimated, and the model was not able to simulate the observed non-zero NO concentrations at night.

A budget analysis of both the box model and p-TOMCAT showed that net chemical production was broadly similar for both models, but there were important differences driven by physical processes. Deposition in the box model drove a net loss of ozone at night, while in the global model this was balanced by advection. The loss was more in line with measurements, though net advection may be important for maintaining the near constant ozone levels that were observed from mid morning to late evening in the measurements.

There are a number of uncertainties that may influence our results, such as the potential importance of OH recycling during isoprene oxidation, the inclusion of monoterpene chemistry, and the impact of hetereogeneous chemistry on NO$_x$. However, our results suggest that the impact of isoprene on ozone is small, and that HO$_2$ and RO$_2$ are relatively well modeled since NO and NO$_2$ are well simulated. This is surprising considering the possible error in the OH simulated by this and other isoprene degradation schemes as described in the literature (e.g. Lelieveld et al., 2008).

Changes in tropical processes, including land use, biogenic VOC emissions, and soil NO$_x$ emissions are important drivers of global change. To assess these changes, global models are generally run at moderate resolutions. In contrast, validation of the global models requires comparison with data representative of much smaller spatial scales. Using a box and global model with the same chemical mechanism, we found that the results were most affected by parameterizations of physical processes.

Supplementary material related to this article is available online at: http://www.atmos-chem-phys.net/10/10607/2010/ acp-10-10607-2010-supplement.pdf.

References

Arnold, S. R., Chipperfield, M. P., and Blitz, M. A.: A three-dimensional model study of the effect of new temperature-dependent quantum yields for acetone photolysis, J. Geophys. Res., 110, D22305, doi:10.1029/2005JD005998, 2005.

Biesenthal, T. A., Bottenheim, J. W., Shepson, P. B., Li, S., and Brickell, P. C.: The chemistry of biogenic hydrocarbons at a rural site in eastern Canada, J. Geophys. Res., 103, 25487–25498, 1998.

Bakwin, P. S., Wofsy, S. C., Fan, S., Keller, M., Trumbore, S. E., and Costa, J. M. D.: Emission of nitric oxide (NO) from tropical forest soils and exchange of NO between the forest canopy and atmospheric boundary layers, J. Geophys. Res., 95, 16755–16764, 1990.

Blake, R. S., Monks, P. S., and Ellis, A. M.: Proton-Transfer Reaction Mass Spectrometry, Chem. Rev., 109, 861–896, 2009.

Brough, N., Reeves, C. E., Penkett, S. A., Stewart, D. J., Dewey, K., Kent, J., Barjat, H., Monks, P. S., Ziereis, H., Stock, P., Huntrieser, H., and Schlager, H.: Intercomparison of aircraft instruments on board the C-130 and Falcon 20 over southern Germany during EXPORT 2000, Atmos. Chem. Phys., 3, 2127–2138, doi:10.5194/acp-3-2127-2003, 2003.

Carver, G. D., Brown, P. D., and Wild, O.: The ASAD atmospheric chemistry integration package and chemical reaction database, Comput. Phys. Commun., 105, 197–215, doi:10.1016/S0010-4655(97)00056-8, 1997.

Cook, P. A., Savage, N. H., Turquety, S., Carver, G. D., O'Connor, F. M., Heckel, A., Stewart, D., Whalley, L. K., Parker, A. E., Schlager, H., Singh, H. B., Avery, M. A., Sachse, G. W., Brune, W., Richter, A., Burrows, J. P., Purvis, A. C., Lewis, A. C., Reeves, C. E., Monks, P. S., Levine, J. G., and Pyle, J. A.: Forest fire plumes over the North Atlantic: p-TOMCAT model simulations with aircraft and satellite measurements from the ITOP/ICARTT campaign, J. Geophys. Res., 112, D10S43, doi:0.1029/2006JD007563, 2007.

Crutzen, P. J.: A discussion of the chemistry of some minor constituents in the stratosphere and troposphere, Pure Appl. Geophys., 106, 1385–1399, doi:10.1007/BF00881092, 1973.

de Gouw, J., Warneke, C., Karl, T., Eerdekens, G., van der Veen, C., and Fall, R.: Sensitivity and specificity of atmospheric trace gas detection by proton-transfer-reaction mass spectrometry, Int. J. Mass Spectrom., 223–224, 365–382, 2003.

Delon, C., Reeves, C. E., Stewart, D. J., Serça, D., Dupont, R., Mari, C., Chaboureau, J.-P., and Tulet, P.: Biogenic nitrogen oxide emissions from soils – impact on NO$_x$ and ozone over West Africa during AMMA (African Monsoon Multidisciplinary Experiment): modelling study, Atmos. Chem. Phys., 8, 2351–2363, doi:10.5194/acp-8-2351-2008, 2008.

Dorsey, J. and Gallagher, M.: Observations of soil NO$_x$ emission from a Southeast Asian rainforest: a technique to assess biological controls, in preparation, 2010.

Duyzer, J. H., Dorsey, J. R., Gallagher, M. W., Pilegaard, K., and Walton, S.: Oxidized nitrogen and ozone interaction with forests. II: Multi-layer process-oriented modelling results and a sensitivity study for Douglas fir, Q. J. Roy. Meteorol. Soc., 130, 1957–1971, 2004.

Forster, P. M. D., Johnson, C. E., Law, K. S., Pyle, J. A., and Shine, K. P.: Further estimates of radiative forcing due to tropospheric ozone changes, Geophys. Res. Lett., 23, 3221–3324, 1996.

Franzblau, E. and Popp, C. J.: Nitrogen oxides produced from lightning, J. Geophys. Res., 94, 11089–11104, 1989.

Fuglestvedt, J. S., Berntsen, T. K., Isaksen, I. S. A., Mao, H., Liang, X.-L., and Wang, W.-C.: Climatic forcing of nitrogen oxides through changes in tropospheric ozone and methane; global 3D model studies, Atmos. Environ., 33, 961–977, doi:10.1016/S1352-2310(98)00217-9, 1999.

Ganzeveld, L. and Lelieveld, J.: Dry deposition parametisation in a chemistry general circulation model and its influence on the distribution of reactive trace gases, J. Geophys. Res., 100, 20999–21012, doi:10.1029/95JD02266, 1995.

Ganzeveld, L., Eerdekens, G., Feig, G., Fischer, H., Harder, H., Königstedt, R., Kubistin, D., Martinez, M., Meixner, F. X., Scheeren, H. A., Sinha, V., Taraborrelli, D., Williams, J., Vilà-Guerau de Arellano, J., and Lelieveld, J.: Surface and boundary layer exchanges of volatile organic compounds, nitrogen oxides and ozone during the GABRIEL campaign, Atmos. Chem. Phys., 8, 6223–6243, doi:10.5194/acp-8-6223-2008, 2008.

Gauss, M., Myhre, G., Pitari, G., Prather, M. J., Isaksen, I. S. A., Berntsen, T. K., Brasseur, G. P., Dentener, F. J., Derwent, R. G., Hauglustaine, D. A., Horowitz, L. W., Jacob, D. J., Johnson, M., Law, K. S., Mickley, L. J., Müller, J. F., Plantevin, P. H., Pyle, J. A., Rogers, H. L., Stevenson, D. S., Sundet, J. K., van Weele, M., and Wild, O.: Radiative forcing in the 21st century due to ozone changes in the troposphere and the lower stratosphere, J. Geophys. Res., 108, D94292, doi:10.1029/2002JD002624, 2003.

Gauss, M., Myhre, G., Isaksen, I. S. A., Grewe, V., Pitari, G., Wild, O., Collins, W. J., Dentener, F. J., Ellingsen, K., Gohar, L. K., Hauglustaine, D. A., Iachetti, D., Lamarque, F., Mancini, E., Mickley, L. J., Prather, M. J., Pyle, J. A., Sanderson, M. G., Shine, K. P., Stevenson, D. S., Sudo, K., Szopa, S., and Zeng, G.: Radiative forcing since preindustrial times due to ozone change in the troposphere and the lower stratosphere, Atmos. Chem. Phys., 6, 575–599, doi:10.5194/acp-6-575-2006, 2006.

Giannakopoulos, C.: Modelling the impact of physical and removal processes on tropospheric chemistry, Ph.D. thesis, University of Cambridge, 1998.

Guenther, A., Hewitt, C. N., Erickson, D., Fall, R., Geron, C., Graedel, T., Harley, P., Klinger, L., Lerdau, M., McKay, W. A., Pierce, T., Scoles, B., Steinbrecher, R., Tallaamraju, R., Taylor, J., and Zimmerman, P.: A global model of natural volatile organic compound emissions, J. Geophys. Res., 100, 8873–8892, 1995.

Hamilton, J. F., Allen, G., Watson, N. M., Lee, J. D., Saxton, J. E., Lewis, A. C., Vaughan, G., Bower, K. N., Flynn, M. J., Crosier, J., Carver, G. D., Harris, N. R. P., Parker, R. J., Remedios, J. J., and Richards, N. A. D.: Observations of an atmospheric chemical equator and its implications for the tropical warm pool region, J. Geophys. Res., 113, D20313, doi:10.1029/2008JD009940, 2008.

Hao, W. M. and Liu, M.-H.: Spatial and temporal distribution of tropical biomass burning, Global Biogeochem. Cy., 8, 495–504, 1994.

Hewitt, C. N., MacKenzie, A. R., Di Carlo, P., Di Marco, C. F., Dorsey, J. R., Evans, M., Fowler, D., Gallagher, M. W., Hopkins, J. R., Jones, C. E., Langford, B., Lee, J. D., Lewis, A. C., Lim, S. F., McQuaid, J., Misztal, P., Moller, S. J., Monks, P. S., Nemitz, E., Oram, D. E., Owen, S. M., Phillips, G. J., Pugh, T. A. M., Pyle, J. A., Reeves, C. E., Ryder, J., Siong, J., Skiba,

U., and Stewart, D. J.: Nitrogen management is essential to prevent tropical oil palm plantations from causing ground-level ozone pollution, P. Natl. Acad. Sci. USA, 106, 18447–18451, doi:10.1073/pnas.0907541106, 2009.

Hewitt, C. N., Lee, J. D., MacKenzie, A. R., Barkley, M. P., Carslaw, N., Carver, G. D., Chappell, N. A., Coe, H., Collier, C., Commane, R., Davies, F., Davison, B., DiCarlo, P., Di Marco, C. F., Dorsey, J. R., Edwards, P. M., Evans, M. J., Fowler, D., Furneaux, K. L., Gallagher, M., Guenther, A., Heard, D. E., Helfter, C., Hopkins, J., Ingham, T., Irwin, M., Jones, C., Karunaharan, A., Langford, B., Lewis, A. C., Lim, S. F., MacDonald, S. M., Mahajan, A. S., Malpass, S., McFiggans, G., Mills, G., Misztal, P., Moller, S., Monks, P. S., Nemitz, E., Nicolas-Perea, V., Oetjen, H., Oram, D. E., Palmer, P. I., Phillips, G. J., Pike, R., Plane, J. M. C., Pugh, T., Pyle, J. A., Reeves, C. E., Robinson, N. H., Stewart, D., Stone, D., Whalley, L. K., and Yin, X.: Overview: oxidant and particle photochemical processes above a south-east Asian tropical rainforest (the OP3 project): introduction, rationale, location characteristics and tools, Atmos. Chem. Phys., 10, 169–199, doi:10.5194/acp-10-169-2010, 2010.

Holton, J. R., Haynes, P. H., McIntyre, M. E., Douglass, A. R., Rood, R. B., and Pfister, L.: Stratosphere-troposphere exchange, Rev. Geophys., 33, 403–439, 1995.

Holtslag, A. and Boville, B.: Local Versus Nonlocal Boundary-Layer Diffusion in a Global Climate Model, J. Climate, 6, 1825–1842, 1993.

Hough, A.: The calculation of photolysis rates for use in global tropospheric modelling studies, AERE Report 13259, At. Energy Res. Estab., Harwell, UK, 1988.

Jaeglé, L., Martin, R. V., Chance, K., Steinberger, L., Kurosu, T. P., Jacob, D. J., Modi, A. I., Yoboué, V., Sigha-Nkamdjou, L., and Galy-Lacaux, C.: Satellite mapping of rain-induced nitric oxide emissions from soils, J. Geophys. Res., 109, D21310, doi:10.1029/2004JD004787, 2004.

Jenkin, M. E. and Clemitshaw, K. C.: Ozone and other secondary photochemical pollutants: Chemical processes governing their formation in the planetary boundary layer, Atmos. Environ., 34, 2499–2527, doi:10.1016/S1352-2310(99)00478-1, 2000.

Jerrett, M., Burnett, R. T., Pope, C. Arden, I., Ito, K., Thurston, G., Krewski, D., Shi, Y., Calle, E., and Thun, M.: Long-Term Ozone Exposure and Mortality, N. Engl. J. Med., 360, 1085–1095, 2009.

Karl, T., Guenther, A., Turnipseed, A., Tyndall, G., Artaxo, P., and Martin, S.: Rapid formation of isoprene photo-oxidation products observed in Amazonia, Atmos. Chem. Phys., 9, 7753–7767, doi:10.5194/acp-9-7753-2009, 2009.

Kasibhatla, P. S.: NO$_y$ from Sub-Sonic Aircraft Emissions: A Global Three-Dimensional Model Study, Geophys. Res. Lett., 20, 1707–1710, 1993.

Kuhn, U., Andreae, M. O., Ammann, C., Araújo, A. C., Brancaleoni, E., Ciccioli, P., Dindorf, T., Frattoni, M., Gatti, L. V., Ganzeveld, L., Kruijt, B., Lelieveld, J., Lloyd, J., Meixner, F. X., Nobre, A. D., Pöschl, U., Spirig, C., Stefani, P., Thielmann, A., Valentini, R., and Kesselmeier, J.: Isoprene and monoterpene fluxes from Central Amazonian rainforest inferred from tower-based and airborne measurements, and implications on the atmospheric chemistry and the local carbon budget, Atmos. Chem. Phys., 7, 2855–2879, doi:10.5194/acp-7-2855-2007, 2007.

Law, K. S. and Pyle, J. A.: Modeling trace gas budgets in the troposphere 1. Ozone and odd nitrogen, J. Geophys. Res., 98, 18377–18400, 1993.

Lelieveld, J., Butler, T. M., Crowley, J. N., Dillon, T. J., Fischer, H., Ganzeveld, L., Harder, H., Lawrence, M. G., Martinez, M., Taraborrelli, D., and Williams, J.: Atmospheric oxidation capacity sustained by a tropical forest, Nature, 452, 737–740, doi:10.1038/nature06870, 2008.

Levy II, H., Moxim, W. J., Klonecki, A. A., and Kasibhatla, P. S.: Simulated tropospheric NO$_X$: Its evaluation, global distribution and individual source contributions, J. Geophys. Res., 104, 26279–26306, 1999.

Lindinger, W., Hansel, A., and Jordan, A.: On-line monitoring of volatile organic compounds at pptv levels by means of proton-transfer-reaction mass spectrometry (PTR-MS) medical applications, food control and environmental research, Int. J. Mass Spectrom. Ion Processes, 173, 191–241, 1998.

Liu, S. C., Trainer, M., Fehsenfeld, F. C., Parrish, D. D., Williams, E. J., Fahey, D. W., Hübler, G., and Murphy, P. C.: Ozone production in the rural troposphere and the implications for regional and global ozone distributions, J. Geophys. Res., 92, 4191–4207, 1987.

Morgenstern, O., Braesicke, P., Hurwitz, M. M., O'Connor, F. M., Bushell, A. C., Johnson, C. E., and Pyle, J. A.: The World Avoided by the Montreal Protocol, Geophys. Res. Lett., 35, L16811, doi:10.1029/2008GL034590, 2008.

Morgenstern, O., Braesicke, P., O'Connor, F. M., Bushell, A. C., Johnson, C. E., Osprey, S. M., and Pyle, J. A.: Evaluation of the new UKCA climate-composition model Part I: The stratosphere, Geoscientific Model Development, 2, 43–57, 2009.

O'Connor, F. M., Johnson, C. E., Morgenstern, O., and Collins, W. J.: Interactions between tropospheric chemistry and climate model temperature and humidity biases, Geophys. Res. Lett., 36, L16801, doi:10.1029/2004JD004787, 2009.

Pearson, G., Davies, F., and Collier, C.: Remote sensing of the tropical rain forest boundary layer using pulsed Doppler lidar, Atmos. Chem. Phys., 10, 5891–5901, doi:10.5194/acp-10-5891-2010, 2010.

Pöschl, U., von Kulhmann, R., Poisson, N., and Crutzen, P. J.: Development and intercomparison of condensed isoprene oxidation mechanisms for global atmospheric modelling, J. Atmos. Chem., 37, 29–52, doi:10.1023/A:1006391009798, 2000.

Prather, M., Ehhalt, D., Dentener, F., Derwent, R., Dlugokencky, E., Holland, E., Isaksen, I., Katima, J., Kirchoff, V., Matson, P., Midgley, P., and Wang, M.: Climate Change 2001: The Scientific Basis, chap. Atmospheric chemistry and greenhouse gases, Cambridge University Press, Cambridge, UK, 239–287, 2001.

Price, C. and Rind, D.: A simple lightning parameterization for calculating global lightning distributions, J. Geophys. Res., 97, 9919–9933, 1992.

Pugh, T. A. M., MacKenzie, A. R., Hewitt, C. N., Langford, B., Edwards, P. M., Furneaux, K. L., Heard, D. E., Hopkins, J. R., Jones, C. E., Karunaharan, A., Lee, J., Mills, G., Misztal, P., Moller, S., Monks, P. S., and Whalley, L. K.: Simulating atmospheric composition over a South-East Asian tropical rainforest: performance of a chemistry box model, Atmos. Chem. Phys., 10, 279–298, doi:10.5194/acp-10-279-2010, 2010.

Saunders, S. M., Jenkin, M. E., Derwent, R. G., and Pilling, M. J.: Protocol for the development of the Master Chemical Mechanism, MCM v3 (Part A): tropospheric degradation of non-aromatic volatile organic compounds, Atmos. Chem. Phys., 3, 161–180, doi:10.5194/acp-3-161-2003, 2003.

Schumann, U. and Huntrieser, H.: The global lightning-induced nitrogen oxides source, Atmos. Chem. Phys., 7, 3823–3907, doi:10.5194/acp-7-3823-2007, 2007.

Sillman, S.: The use of NO$_y$, H$_2$O$_2$, and HNO$_3$ as indicators for ozone-NO$_x$-hydrocarbon sensitivity in urban locations, J. Geophys. Res., 100, 14175–14188, 1995.

Sillman, S., Logan, J. A., and Wofsy, S. C.: The sensitivity of ozone to nitrogen oxides and hydrocarbons in regional ozone episodes, J. Geophys. Res., 95, 1837–1851, 1990.

Steinkamp, J., Ganzeveld, L. N., Wilcke, W., and Lawrence, M. G.: Influence of modelled soil biogenic NO emissions on related trace gases and the atmospheric oxidizing efficiency, Atmos. Chem. Phys., 9, 2663–2677, doi:10.5194/acp-9-2663-2009, 2009.

Stevenson, D. S., Dentener, F. J., Schultz, M. G., Ellingsen, K., van Noije, T. P. C., Wild, O., Zeng, G., Amann, M., Atherton, M., Bell, N., Bergmann, D. J., Bey, I., Bulter, T., Cofala, J., Collins, W. J., Derwent, R. G., Doherty, R. M., Drevet, J., Eskes, H. J., Fiore, A. M., Gauss, M., Hauglustaine, D. A., Horowitz, L. W., Isaksen, I. S. A., Krol, M. C., Lamarque, J.-F., Lawrence, M. G., Montanaro, V., Müller, J. F., Pitari, G., Prather, M. J., Pyle, J. A., Rast, S., Rodriguez, J. M., Sanderson, M. G., Savage, N. H., Shindell, D. T., Strahan, S. E., Sudo, K., and Szopa, S.: Multimodel ensemble simulations of present-day and near-future tropospheric ozone, J. Geophys. Res., 111, D08301, doi:10.1029/2005JD006338, 2006.

Stockwell, D. Z., Giannakopoulos, C., Plantevin, P.-H., Carver, G. D., Chipperfield, M. P., Law, K. S., Pyle, J. A., Shallcross, D. E., and Wang, K. Y.: Modelling NO$_X$ from lightning and its impact on global chemical fields, Atmos. Environ., 33, 4477–4493, doi:10.1016/S1352-2310(99)00190-9, 1999.

Toenges-Schuller, N., Stein, O., Rohrer, F., Wahner, A., Richter, A., Burrows, J. P., Beirle, S., Wagner, T., Platt, U., and Elvidge, C. D.: Global distribution pattern of anthropogenic nitrogen oxide emissions: Correlation analysis of satellite measurements and model calculations, J. Geophys. Res., 111, D05312, doi:10.1029/2005JD006068, 2006.

Trainer, M., Buhr, M. P., Curran, C. M., Fehsenfeld, F. C., Hsie, E. Y., Liu, S. C., Norton, R. B., Parrish, D. D., Williams, E. J., Gandrud, B. W., Ridley, B. A., Shetter, J. D., Allwine, E. J., and Westberg, H. H.: Observations and modeling of the reactive nitrogen photochemistry at a rural site, J. Geophys. Res., 96, 3045–3063, 1991.

van Dingenen, R., Dentener, F. J., Raes, F., Krol, M. C., Emberson, L., and Cofala, J.: The global impact of ozone on agricultural crop yields under current and future air quality legislation, Atmos. Environ., 43, 604–618, 2009.

Wild, O.: Modelling the global tropospheric ozone budget: exploring the variability in current models, Atmos. Chem. Phys., 7, 2643–2660, doi:10.5194/acp-7-2643-2007, 2007.

Wilkins, C. K., Clausen, P. A., Wolkoff, P., Larsen, S., Hammer, M., Larsen, K., Hansen, V., and Nielsen, G. D.: Formation of strong airway irritants in mixtures of isoprene/ozone and isoprene/ozone/nitrogen dioxide, Environ. Health Persp., 109, 937–941, 2001.

Yienger, J. J. and Levy II, H.: Empirical model of global soil-

biogenic NO$_x$ emissions, J. Geophys. Res., 100, 11 477–11 464, 1995.

Young, P. J., Arneth, A., Schurgers, G., Zeng, G., and Pyle, J. A.: The CO$_2$ inhibition of terrestrial isoprene emission significantly affects future ozone projections, Atmos. Chem. Phys., 9, 2793–2803, doi:10.5194/acp-9-2793-2009, 2009.

Zeng, G., Pyle, J. A., and Young, P. J.: Impact of climate change on tropospheric ozone and its global budgets, Atmos. Chem. Phys., 8, 369–387, doi:10.5194/acp-8-369-2008, 2008.

Zhang, L., Brook, J. R., and Vet, R.: A revised parameterization for gaseous dry deposition in air-quality models, Atmos. Chem. Phys., 3, 2067–2082, doi:10.5194/acp-3-2067-2003, 2003.